

Article

Adsorption Behavior of Lead Ions from Wastewater on Pristine and Aminopropyl-Modified Blast Furnace Slag

Yali Wang^{1,2}, Huining Li^{1,2}, Suping Cui^{1,2} and Qi Wei^{1,2,*}

¹ Faculty of Materials and Manufacturing, Beijing University of Technology, 100 Pingleyuan, Chaoyang District, Beijing 100124, China; wangyali1978@bjut.edu.cn (Y.W.); lhn779804000@126.com (H.L.); cuisuping@bjut.edu.cn (S.C.)

² The Key Laboratory of Advanced Functional Materials, Ministry of Education of China, 100 Pingleyuan, Chaoyang District, Beijing 100124, China

* Correspondence: qiwei@bjut.edu.cn

Abstract: The potential possibility of blast furnace slag as a low-cost adsorbent to remove lead ions from wastewater was investigated in detail in the present work. Both single factor experiment and orthogonal experiment were performed to reveal the effect of pH, adsorption temperature, contact time and initial concentration of lead ions on the adsorption performance of pristine slag. In order to make clear the correlation between the lead ion adsorption performance and the structure of slag, solid state nuclear magnetic resonance (NMR) was conducted to reveal the network structure and X-ray fluorescence (XRF) was used to calculate the nonbridging oxygen in the network-forming tetrahedra. For the purpose of improving the adsorption performance, γ -aminopropyltriethoxysilane (APTES) was adopted to modify the slag via post-grafting method. The results show that the slag is predominately composed of SiO_2 , Al_2O_3 , CaO and MgO , exhibiting an amorphous network structure based on SiO_4 and AlO_4 tetrahedra. The conditions for adsorption can be optimized as follows: a pH of 7, an adsorption temperature of 60 °C, a contact time of 120 min and an initial lead ion concentration of 40 $\text{mg}\cdot\text{L}^{-1}$. Under the optimal conditions, a removal rate of 99.98% and an adsorption capacity of 49.99 $\text{mg}\cdot\text{g}^{-1}$ are obtained for the pristine slag. The adsorption complies with the Langmuir model thermodynamically and conforms to the pseudo-second order model kinetically. It is noted that aminopropyl-modification has considerably enhanced the removal rate of lead ions from 20.71 to 64.32% and the adsorption capacity from 29.01 to 96.48 $\text{mg}\cdot\text{g}^{-1}$ since amino groups ($-\text{NH}_2$) are more inclined to form a complex with lead ions than hydroxyl groups due to the higher nucleophilicity of amino groups than that of hydroxyl groups. However, it is necessary to develop more low-cost modification agents in the future work.



Citation: Wang, Y.; Li, H.; Cui, S.; Wei, Q. Adsorption Behavior of Lead Ions from Wastewater on Pristine and Aminopropyl-Modified Blast Furnace Slag. *Water* **2021**, *13*, 2735. <https://doi.org/10.3390/w13192735>

Academic Editor: Antonio Zuorro

Received: 13 August 2021

Accepted: 25 September 2021

Published: 2 October 2021

Publisher's Note: MDPI stays neutral with regard to jurisdictional claims in published maps and institutional affiliations.



Copyright: © 2021 by the authors. Licensee MDPI, Basel, Switzerland. This article is an open access article distributed under the terms and conditions of the Creative Commons Attribution (CC BY) license (<https://creativecommons.org/licenses/by/4.0/>).

Keywords: blast furnace slag; lead ions; adsorption; surface modification; aminopropyl groups

1. Introduction

As one of the most toxic and extremely hazardous heavy metals, lead causes serious damage to the kidney, liver, nervous, reproductive and gastrointestinal systems of humans [1,2]. In general, Lead pollution primarily derives from wastewater produced in metallurgy, mining, battery manufacturing, electroplating, etc. [3,4]. In order to avoid huge harm to the environment, it is critically necessary to remove lead ions from wastewater prior to its discharge. In the past decades, various techniques have been developed and employed for removing toxic heavy metal ions from wastewater, including but not limited to chemical precipitation [5], ion exchange [6], membrane separation [7], reverse osmosis [8], phytoremediation [9], adsorption [10–14], among others. Amongst these techniques, adsorption has received increasing attention due to its ease of operation and abundance of adsorbents [15–17]. Zeolites, ordered mesoporous silica, activated carbon, clay minerals [18], etc. are considerably effective for metal ions removal by adsorption due to their high porosity and surface area, but most of these adsorbents are quite expensive

because of the complex synthesis process, involving high energy consumption and large depletion of raw material sources [10], thus limiting their widespread use in wastewater treatment. Recently, various industrial or agricultural wastes, for instance, sludge, blast furnace slag, flue dust, red mud, banana peel, soybean hull, spent coffee grounds etc., have been investigated for the adsorption of heavy metals from wastewater [14,17,19–22].

Blast furnace slag is a kind of industrial byproduct from steel plants. Currently, slag has been successfully utilized in large scale as raw materials or fillers in cement production, road construction and asphalts. A large amount of slag that cannot be recycled or recovered is landfilled, which leads to a major environmental issue [1,23]. In recent years, numerous researchers have explored the possibility that using slag as an alternative adsorbent for the removal of heavy metals from wastewater [10,16,23]. The removal characteristics of different metal ions using different slags have been investigated in terms of adsorption isotherms/kinetics, and various removal mechanisms have also been proposed [2,24].

Previous literature has demonstrated that surface modification by grafting functional groups onto the surface of adsorbents through chemical reaction achieves higher metal ions removal efficiency [25,26]. Deng et al. introduced amine groups on the surfaces of polyacrylonitrile fibers (PANFs) through a simple one-step reaction of PANFs with diethylenetriamine solution [27]. The aminated polyacrylonitrile fibers (APANFs) had significantly higher adsorption capacities for both lead and copper ions than PANFs. Amino-functionalized Fe_3O_4 @mesoporous SiO_2 core-shell composite microspheres, magnesium silicate hollow microspheres and multiwall carbon nanotubes/iron oxides nanocomposites for enhanced lead ion removal were synthesized by Tang et al. [28], Zou et al. [29] and Ji et al. [30], respectively. Zhu et al. reported that surface-ion imprinted polymer exhibits excellent affinity and high selectivity toward metal ions [31]. In particular, the amino group has been proved to be one of the most effective chelating groups for the adsorption or removal of heavy metal ions from aqueous solutions. However, rare reports have focused on the surface modification of slag with amino group for heavy ions adsorption, so far.

It is well known that slag is typically composed of SiO_2 , CaO , Al_2O_3 , Fe_2O_3 and MgO . However, compared to the chemical composition, the network structure of the slag, especially the nonbridging oxygen in the network-forming tetrahedra, which play a crucial role in the complexation of lead ions with pristine slag, has rarely been investigated previously.

In the present work, the chemical composition, phase composition, structure, morphology and, more importantly, the lead ion adsorption behavior of the blast furnace slag are investigated in detail; γ -aminopropyltriethoxysilane (APTES) is adopted to modify the slag via post-grafting method in order to enhance the adsorption performance of the slag. An adsorption mechanism is also proposed. Emphasis is placed on using solid state nuclear magnetic resonance (NMR) to reveal the network structure of slag. Solid state NMR is a powerful technique to analyze the structure of various types of materials, especially the local structure of the amorphous materials such as blast furnace slag, which cannot be clearly identified by sole X-ray diffraction (XRD) measurement. In addition, X-ray fluorescence (XRF) data are used to calculate the nonbridging oxygen in the network-forming tetrahedra. To date, the concentrated study on the local structure of slag by a combination of solid state NMR and XRF and the discussion with respect to surface modification have not been reported previously and it represents the major novelty of the present work. The practical application of this work is to provide a strategy to reveal the structure of slag and enhance its removal performance of lead ions from wastewater.

2. Materials and Methods

2.1. Chemicals

Blast furnace slag was provided by a steel plant in China. Lead nitrate ($\text{Pb}(\text{NO}_3)_2$, A.R.) was purchased from Shanghai Aladdin Bio-Chem Technology Co., Ltd. (Shanghai, China). Concentrated nitric acid (HNO_3 , 65%), sodium hydroxide (NaOH , A.R.) and absolute alcohol (EtOH , A.R.) were obtained from Beijing Chemical Works (Beijing, China); γ -aminopropyltriethoxysilane (APTES) was purchased from JiuDing Chemical Technology

Co., Ltd. (Shanghai, China). Deionized water (H_2O) with a resistivity close to $18 \Omega \text{ cm}$ was produced by a water purification system (Ulupure, Chengdu, China). All chemicals except blast furnace slag were used as received without further purification. The lead ion solution was prepared by dissolving a certain amount of $Pb(NO_3)_2$ in deionized water.

2.2. Adsorbent Preparation

The slag was washed repeatedly (once for 1 h) using deionized water until the supernatant reached a pH of 7. After drying at $100 \text{ }^\circ\text{C}$ for 24 h, the slag was processed by a sieve to remove coarse particles that were larger than 400 mesh. The pretreated slag was denoted as pristine slag and used for characterization, adsorption or further surface modification.

The surface modification was carried out by a post-grafting approach with APTES as modification agent [28,29]. A certain amount of APTES was dissolved in ethanol and then ultrasonically treated for 15 min to obtain a modified solution with different mass ratios of APTES in EtOH solution (Table 1). Prior to surface modification, the pretreated slag (pristine slag) was cleaned by ethanol and deionized water alternately. After vacuum-drying at $120 \text{ }^\circ\text{C}$ for 12 h, the slag (2 g) was added into the modification solution (50 mL) and stirred at different temperatures for set times (Table 1). Finally, the slag was filtered, washed with ethanol to remove the residual unreacted APTES and then dried at $110 \text{ }^\circ\text{C}$ for 24 h.

Table 1. List of the factors and their levels for surface modification.

Factors	Levels
Mass ratio of APTES in EtOH solution (%)	5, 10, 15, 20, 25, 30, 35, 40
Modification time (h)	6, 12, 24, 36, 48
Modification temperature ($^\circ\text{C}$)	20, 30, 40, 50

2.3. Adsorbent Characterization

The chemical composition of slag was analyzed by X-ray fluorescence (XRF-1800, Shimadzu, Kyoto, Japan). The phase composition was identified by X-ray diffractometer (XRD-7000, Shimadzu, Kyoto, Japan) using $\text{Cu K}\alpha 1$ radiation with a scanning rate of $2^\circ/\text{min}$. Solid state ^{29}Si and ^{27}Al magic angle spinning nuclear magnetic resonance (^{29}Si and ^{27}Al MAS NMR) spectra were measured by a 400 MHz Bruker Avance III WB NMR spectrometer (Rheinstetten, Germany) using a 4 mm Bruker CP/MAS probe with a spinning rate of 9 kHz. The chemical shifts of ^{29}Si and ^{27}Al were referenced to tetramethylsilane (TMS) and an aqueous solution of $\text{AlCl}_3 \cdot 6\text{H}_2\text{O}$, respectively. The surface atomic composition of slag was determined using X-ray photoelectron spectroscopy (XPS, Escalab 250Xi, Thermo Fisher, Waltham, MA, USA) equipped with a monochromatic $\text{Al K}\alpha$ source radiation (1486.6 eV) and $500 \mu\text{m}$ spot size. The pore structure of the slag was detected by N_2 adsorption–desorption at 77 K conducted on the specific surface area and pore size analyzer (BSD-PS (M), BeiShiDe Instrument Technology (Beijing), Co., Ltd., Beijing, China). Prior to measurement, the samples were degassed at $100 \text{ }^\circ\text{C}$ for 12 h to remove moisture or impurities. The morphology was observed by a scanning electron microscope (SEM, JSM 6500, Tokyo, Japan). The samples were sputtered with gold prior to imaging. The concentration of lead ions in solution was determined by an inductive coupled plasma emission spectrometer (Optima 7000DV, PerkinElmer, Waltham, MA, USA).

2.4. Adsorption Experiments

A set amount of pristine or modified slag (0.1 g) was added to 50 mL aqueous solutions with different lead ion concentrations and pH and stirred for different times under different temperatures. Afterward, the supernatant was filtered through a membrane with a pore size of $0.45 \mu\text{m}$, and the concentration of lead ions in the filtrate was detected. The lead

ion removal rate (η , %) and the adsorption capacity (q_t , $\text{mg}\cdot\text{g}^{-1}$) at time t were calculated according to Equations (1) and (2) [16], respectively:

$$\eta(\%) = \frac{C_0 - C_t}{C_0} \times 100\% \quad (1)$$

$$q_t = \frac{(C_0 - C_t)V}{m} \quad (2)$$

where C_0 ($\text{mg}\cdot\text{L}^{-1}$) represents the initial concentration of lead ions in the solution, C_t ($\text{mg}\cdot\text{L}^{-1}$) denotes the concentration of lead ions at time t , V (L) refers to the volume of solution and m (g) is the mass of slag.

For the single factor analysis, the effect of pH, adsorption temperature, contact time and initial concentration of lead ions on the removal rate and adsorption capacity was investigated in detail by varying one factor while fixing the other three factors. The values of the single factors used in the experiments are listed in Table 2.

Table 2. List of the factors and their levels for single factor analysis.

Factors	Levels
pH	2, 5, 7, 9, 11
Temperature ($^{\circ}\text{C}$)	20, 30, 40, 50, 60
Contact time (min)	10, 20, 30, 60, 90, 120, 150, 180, 240, 300
Initial lead ions concentration ($\text{mg}\cdot\text{L}^{-1}$)	20, 40, 60, 80, 100, 150, 200, 300

For the orthogonal experimental study, experiments were performed according to the orthogonal array L_9 (3^4) that are listed in Table 3. Two indices in the orthogonal experiment, removal rate and adsorption capacity, were measured according to the same procedure that was used in the single factor experiments.

Table 3. List of factors and levels for the orthogonal experimental study.

Levels	Factor A	Factor B	Factor C	Factor D
	pH	Temperature ($^{\circ}\text{C}$)	Contact Time (min)	Initial Concentration ($\text{mg}\cdot\text{L}^{-1}$)
1	2	20	30	40
2	5	40	120	100
3	7	60	240	300

The adsorption conditions for the modified slag prepared under different conditions follow: modified slag amount of 0.1 g, simulated wastewater volume of 50 mL, initial lead ion concentration of $200 \text{ mg}\cdot\text{L}^{-1}$, contact time of 60 min, pH of 6 and adsorption temperature of 20°C . The adsorption performance of the modified slag prepared under the optimal condition was compared to that of the pristine slag under these same conditions, except for an initial lead ion concentration of $300 \text{ mg}\cdot\text{L}^{-1}$.

3. Results and Discussion

3.1. Characterization of Slag

Table 4 lists the chemical composition (in mole percentage) of the pristine slag detected by XRF. The slag is mainly composed of CaO , SiO_2 , Al_2O_3 and MgO , accounting for more than 99% of the composition. As depicted in Figure 1, only a rather broad peak is observed in the XRD pattern, indicating that the slag is amorphous. In fact, the slag can be approximately considered as a type of Mg-substituted calcium aluminosilicate glass (MCAS) [32]. In order to further reveal the structure of slag, both ^{29}Si MAS NMR and ^{27}Al MAS NMR measurements were conducted and the results are exhibited in Figure 2. As shown in the ^{29}Si MAS NMR spectrum, in the range from -50 to -130 ppm there is

a broad resonance covering the chemical shift region of the silicon atoms in the Q_n , i.e., $Si((OSi)_n(OH)_{4-n})$, $n = 0\sim 4$ and $Q_n(mAl)$, i.e., $Si((OSi)_{n-m}(OAl)_m(OH)_{4-n})$, $m = 0\sim n$ environments [33–35]. For the ^{27}Al MAS NMR spectrum, the resonance at 59 ppm is attributed to the aluminum atoms in $AlO_4(4Si)$ tetrahedra [33–35]. A bridging SiO_4 tetrahedra is required to be located between two neighboring AlO_4 tetrahedra; in other words, nonbridging oxygens (NBOs, for example, the oxygen in OH group) are associated with SiO_4 rather than AlO_4 tetrahedra [32]. The Ca^{2+} and Mg^{2+} cations play dual role in the slag structure. On the one hand, as network modifiers, they break the Si-O-Si bonds and create nonbridging oxygens. On the other hand, they balance the negative charge generated by the substitution of Si by Al as charge compensators [32]. The number of NBO per network-forming tetrahedra calculated according to the XRF data is 1.11 for the slag in this work [32]. It is generally believed that the nonbridging oxygens behave as binding sites for heavy metal ion adsorption [11,15,36].

Table 4. Chemical composition of pristine slag (mol%).

SiO ₂	CaO	Al ₂ O ₃	MgO	SO ₃	TiO ₂	Na ₂ O	Fe ₂ O ₃	MnO	K ₂ O	SrO	NBO *
51.03	34.88	5.69	5.62	1.25	0.64	0.35	0.14	0.19	0.19	0.02	1.11

* NBO: number of nonbridging oxygen per network-forming tetrahedra, calculated according to the equation $NBO/T = (2[Ca] + 2[Mg] - [Al]) / ([Si] + [Al])$.

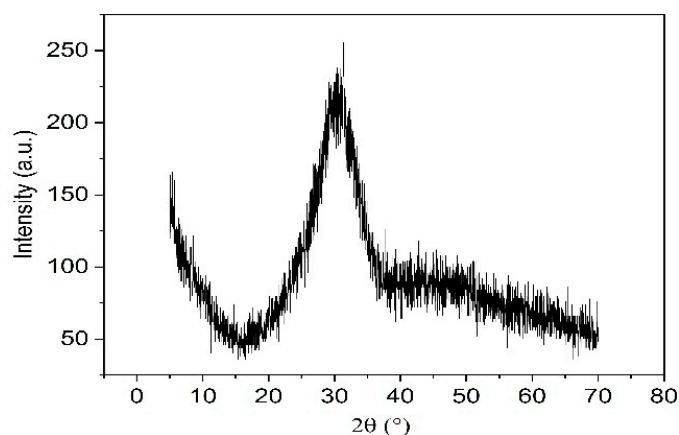


Figure 1. XRD pattern of pristine slag.

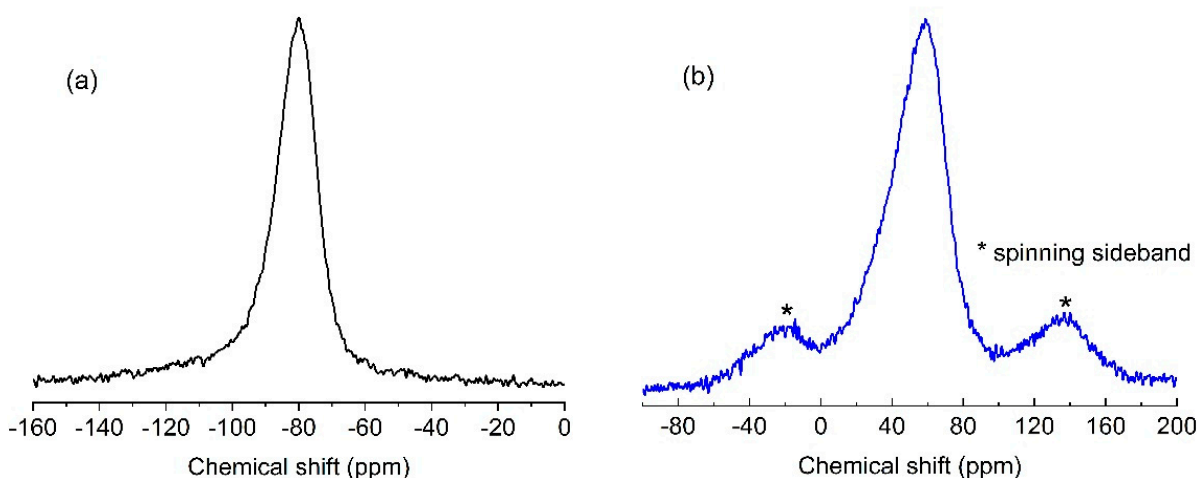


Figure 2. Solid state ^{29}Si (a) and ^{27}Al (b) MAS NMR spectra of pristine slag.

Figure 3 reveals the elemental compositions of the pristine and aminopropyl-modified slag determined by XPS. The XPS data reflect the composition of the topmost surface (usually several nanometers) of the samples [37]. Figure 3a exhibits the presence of the main constituent elements (Si, Al, Ca, Mg and O) in the pristine slag. The signal of C, which is not intrinsically a constituent element of slag, originates from the adsorption of C species in the atmosphere. For the aminopropyl-modified slag (Figure 3b), additional peak of N is detected at a binding energy of 399 eV [38,39], and the elemental concentration of C increases from 18.36% for the pristine slag to 26.4% (Table 5). This observation confirms that the aminopropyl groups were successfully incorporated onto the surface of slag.

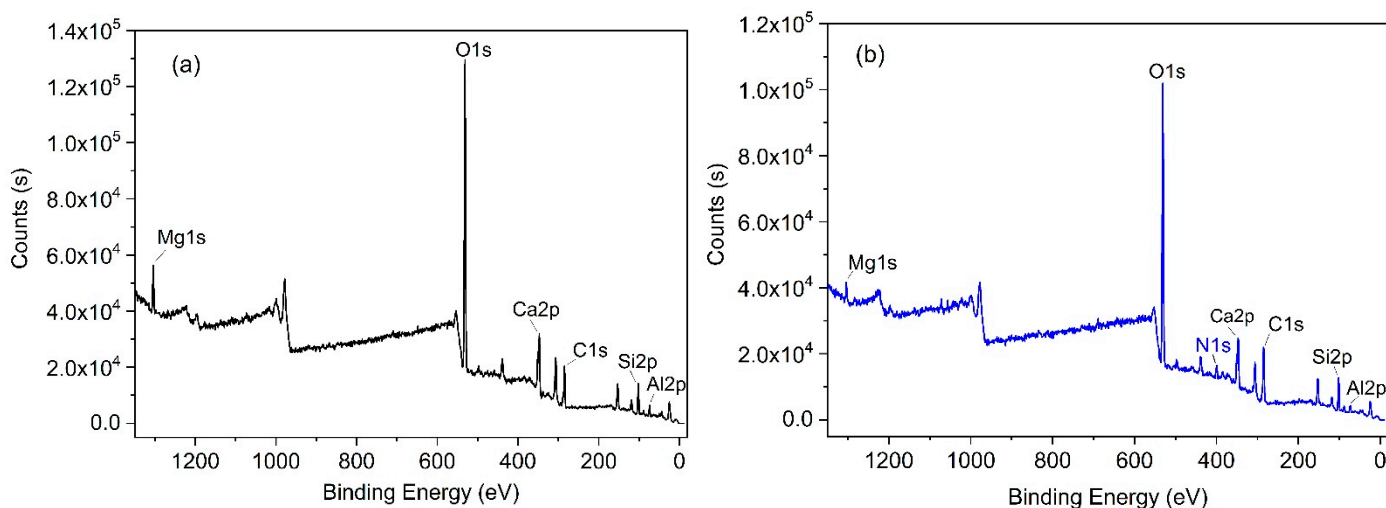


Figure 3. XPS spectra of pristine (a) and aminopropyl-modified (b) slag.

Table 5. Elemental compositions (atomic %, without hydrogen) of slag determined by XPS.

Sample	O	C	Si	Mg	Ca	N	Al
Pristine slag	52.10	18.36	12.27	3.62	6.40	0.00	7.25
Modified slag	45.57	26.40	11.75	2.02	5.06	3.94	5.26

Figure 4 exhibits the N_2 adsorption–desorption isotherms of the pristine slag treated with aqueous solution with different pH for an hour and that of the aminopropyl-modified slag. Table 6 summarizes the textural parameters of the samples. All samples exhibit a type II isotherm, indicating that the slag is intrinsically nonporous [40]. The BET surface area ranging from 0.746 to 0.898 $m^2 \cdot g^{-1}$ and the pore volume from 0.0032 to 0.0046 $cm^3 \cdot g^{-1}$ of the slag are negligible compared to those of a typical porous solid such as SBA-15, which has a BET surface area of 633–816 $m^2 \cdot g^{-1}$ and a pore volume of 0.7–1.41 $cm^3 \cdot g^{-1}$ [41]. It is observed that all isotherms overlap with each other, suggesting that the aminopropyl-modification does not obviously damage the surface or change the porosity of the slag.

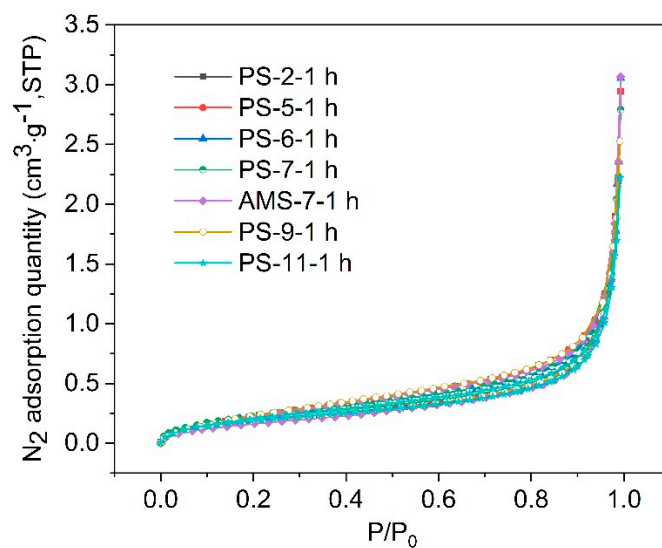


Figure 4. N₂ adsorption–desorption isotherms of the slag. Note: the legend means that the pristine slag (PS) and the aminopropyl-modified slag (AMS) were treated in the aqueous solution with a pH of 2, 5, 6, 7, 9 and 11 for 1 h, respectively, at room temperature.

Table 6. The textual parameters of the slag.

Sample	BET Surface Area (m ² ·g ⁻¹)	Pore Volume (cm ³ ·g ⁻¹)
PS-2-1 h	0.898	0.0046
PS-5-1 h	0.752	0.0039
PS-6-1 h	0.765	0.0038
PS-7-1 h	0.808	0.0038
AMS-7-1 h	0.661	0.0039
PS-9-1 h	0.750	0.0037
PS-11-1 h	0.746	0.0032

Note: the sample symbols mean that the pristine slag (PS) and the aminopropyl-modified slag (AMS) were treated in the aqueous solution with a pH of 2, 5, 6, 7, 9 and 11 for 1 h, respectively, at room temperature.

The SEM images in Figure 5 show that the slag consists of irregularly shaped particles with a rough surface and a size ranging from several microns to more than 20 microns.

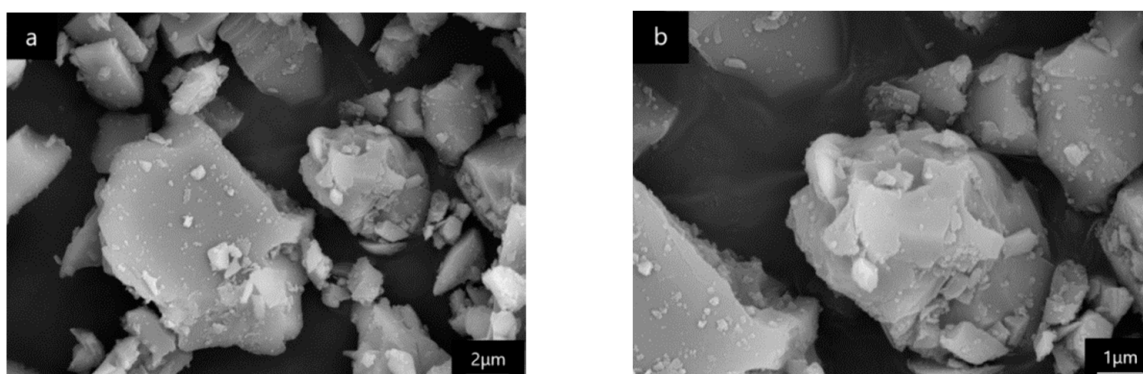
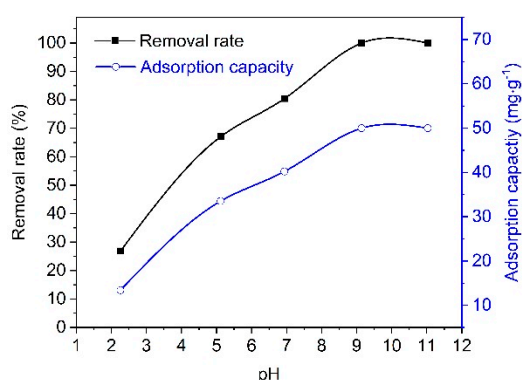


Figure 5. SEM images of pristine slag. (b) is the close-up of (a).

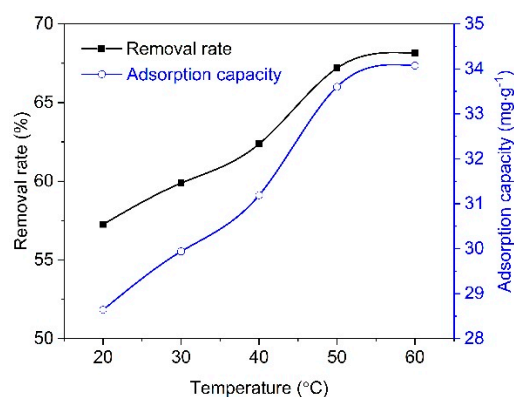
3.2. Lead Ions Adsorption on Pristine Slag

3.2.1. Single Factor Analysis

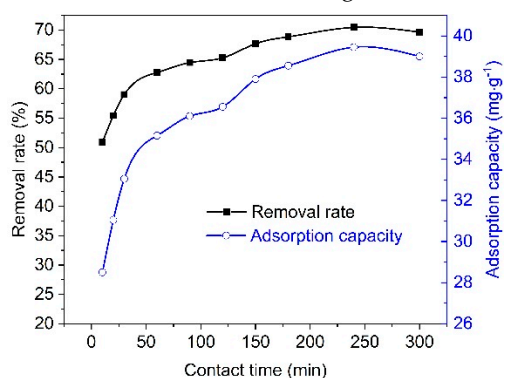
The removal rate and adsorption capacity were investigated under pH ranging from 2 to 11 with an interval of 2. As shown in Figure 6a, the removal rate increases with increasing pH until a value of 9, at which point 100% is obtained. The effect of pH on adsorption capacity is similar to that on removal rate. The adsorption capacity reaches a maximum value of $49.98 \text{ mg}\cdot\text{g}^{-1}$ at a pH of 9 and then remains constant at higher pH. The dependence of removal efficiency on pH may be partially attributed to the concentration of H^+ present in the solution. At lower pH, the concentration of H^+ is high and a large amount of H^+ competes with Pb^{2+} for adsorption sites [12], thus leading to a low Pb^{2+} uptake for the slag. At higher pH the competing effect of H^+ weakens due to the decrease of H^+ concentration. Hence, more free binding sites on the slag surface are available for the positively charged lead ions, thus resulting in a higher removal rate of lead ions. Additionally, chemical precipitation takes place at higher pH via the reaction of Pb^{2+} with OH^- , whose concentration tends to increase under more alkaline condition. At a pH of 9, the residual Pb^{2+} is completely removed by the formation of $\text{Pb}(\text{OH})_2$ precipitate. In order to reduce the precipitation effect and avoid the dissolution of SiO_2 in alkaline solution, a pH of 6 was selected in the further single factor experiments unless otherwise stated. As shown in Figure 4 and Table 6, the slag remains intact after submitting to the aqueous solution with different pH for the adsorption for 1 h, suggesting that the surface of the slag is not destroyed significantly by the acidic or alkaline solution.



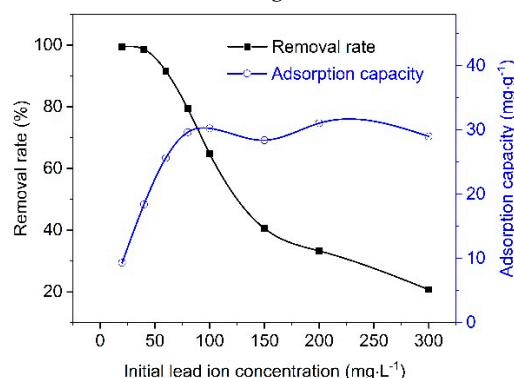
(a) Temperature: $20 \text{ }^\circ\text{C}$; contact time: 60 min; initial lead ion concentration: $120 \text{ mg}\cdot\text{L}^{-1}$



(b) pH: 6; contact time: 60 min; initial lead ion concentration: $120 \text{ mg}\cdot\text{L}^{-1}$



(c) pH: 6; temperature: $20 \text{ }^\circ\text{C}$; initial lead ion concentration: $120 \text{ mg}\cdot\text{L}^{-1}$



(d) pH: 6; temperature: $20 \text{ }^\circ\text{C}$; contact time: 60 min

Figure 6. Removal rate and adsorption capacity of lead ions by pristine slag under different pH values (a), temperature (b), contact time (c) and initial concentration (d).

As depicted in Figure 6b, the removal rate and adsorption capacity increase steadily from 20 to $50 \text{ }^\circ\text{C}$, but the tendency becomes much less pronounced from 50 to $60 \text{ }^\circ\text{C}$.

This indicates that the adsorption process is endothermic in nature [42], especially for the temperature range from 20 to 50 °C. It is generally believed that higher temperature is in favor of the motion of lead ions in the solution, thus enhancing the opportunity for the collision of lead ions with the binding sites. It is possible that at a temperature of 50 °C, the binding sites have been almost completely occupied by lead ions, so that the adsorption is no more reinforced considerably at temperatures higher than 50 °C.

Figure 6c shows the effect of contact time on the removal rate and adsorption capacity of pristine slag. A rapid increase for both removal rate and adsorption capacity can be observed in the first 180 min, and then the increase slows with further increasing contact time. The equilibrium adsorption can be considered to occur at the contact time of 180 min with an adsorption capacity of 38.55 mg·g⁻¹. The fast adsorption during the initial stage is explained by the abundant free binding sites available for adsorption.

Figure 6d displays the effect of initial lead ion concentrations on the removal rate and adsorption capacity of slag. It can be seen that at a low initial concentration (≤ 40 mg·L⁻¹) lead ions can be almost completely removed by the slag since there are abundant free binding sites for lead ions on the slag surface. For the range from 40 to 80 mg·L⁻¹, the adsorption capacity increases with increasing initial lead ion concentration, but the removal rate decreases from nearly 100 to 80%. The increase of adsorption capacity is probably ascribed to the driving force that is initiated by the initial concentration to reduce the mass transfer resistance [12,43]. The reverse trend for the removal rate indicates that some lead ions do not interact with the binding sites that are available for adsorption. As the initial concentration further rises to 100 mg·L⁻¹, adsorption saturation takes place since the binding sites are totally occupied by the lead ions. The removal rate drops to 60% due to the presence of residual lead ions in the solution that have no opportunity to combine with the binding sites. This observation implies that the pristine slag is less effective for lead ion removal at high initial concentration. In order to promote the removal effectiveness at high lead ion concentration, the saturated adsorption capacity should be enhanced. Desorption is expected to occur simultaneously with adsorption if the affinity between the binding sites and lead ions is weak. Hence, a strategy to enhance the interaction between slag surface and lead ions is necessarily required.

In summary, the optimal operating conditions originated from the single factor analysis list as follows: a pH of 6, a temperature of 50 °C, a contact time of 240 min and an initial lead ion concentration of 100 mg·L⁻¹.

3.2.2. Orthogonal Experimental Study

Table 7 lists the design of orthogonal experiments and the experimental results for two indices: removal rate and adsorption capacity. Range analysis is conducted to determine the influence degree and optimal level of each factor for the removal rate and adsorption capacity; the results are listed in Table 8. The influence degree of factors for both indices decreases in the order: D > A > C > B (Table 8). The initial lead ion concentration has the largest R value, indicating that it affects the removal efficiency most remarkably. The pH comes in second, followed by temperature and contact time. The temperature and contact time have a similar R value, suggesting that their effect on the indices differs slightly. Taking the levels into account, the optimal combination for both removal rate and adsorption capacity is D1A3C3B3, but this combination does not appear in the orthogonal array (Table 7). It is found that a similar combination of D1A3C2B3 appears in the orthogonal array and the experiment based on this combination results in the highest removal rate (99.98%) and the largest adsorption capacity (49.99 mg·g⁻¹). Therefore, D1A3C2B3, namely, a pH of 7, a temperature of 60 °C, a contact time of 120 min and an initial lead ion concentration of 40 mg·L⁻¹, can be considered as the optimal experiment conditions in this work. It is noted that the optimal operating conditions derived from the orthogonal study differs from those determined by the single factor experiments. However, such differences are reasonable and acceptable since the orthogonal experimental study considers the influence factors comprehensively. After treatment by the slag under the optimal conditions,

the lead ion concentration in wastewater is less than 1 mg·L⁻¹, close to the emission standards of pollutants for lead and zinc industry (GB 25466-2010).

Table 7. Orthogonal experiment design and experimental results.

Combination	Factor A	Factor B	Factor C	Factor D	Removal Rate (%)	Adsorption Capacity (mg·g ⁻¹)
A1B1C1D1	2	20	30	40	69.61	34.81
A1B2C2D2	2	40	120	100	45.96	22.98
A1B3C3D3	2	60	240	300	14.95	7.48
A2B1C2D3	5	20	120	300	18.04	9.02
A2B2C3D1	5	40	240	40	98.45	49.22
A2B3C1D2	5	60	30	100	69.31	34.66
A3B1C3D2	7	20	240	100	76.69	38.35
A3B2C1D3	7	40	30	300	36.48	18.24
A3B3C2D1	7	60	120	40	99.98	49.99

Note: A, B, C and D represent pH, temperature (°C), contact time (min) and initial lead ion concentration (mg·L⁻¹), respectively.

Table 8. Range analysis of removal rate and adsorption capacity.

	Removal Rate				Adsorption Capacity			
	Factor A	Factor B	Factor C	Factor D	Factor A	Factor B	Factor C	Factor D
k1	43.51	54.78	58.47	89.35	21.76	27.39	29.24	44.67
k2	61.93	60.30	54.66	63.99	30.97	30.15	27.33	32.00
k3	71.05	61.42	63.36	23.16	35.53	30.71	31.68	11.58
R	27.55	6.64	8.70	66.19	13.77	3.32	4.35	33.09
Optimum level	7	60 °C	240 min	40 mg·L ⁻¹	7	60 °C	240 min	40 mg·L ⁻¹
Rank for the influence degree of factors on both removal rate and adsorption capacity: D > A > C > B								

Note: k1, k2 and k3 represent the average removal rate and adsorption capacity of each factor at level 1, 2 and 3, respectively. R value for each factor is the difference between the maximum and minimum value of k.

3.2.3. Adsorption Isotherms

Three typical adsorption models, the Langmuir Equation (3), the Freundlich Equation (4) and the Dubinin–Radushkevich (D–R) Equation (5) are used to fit the adsorption data [21,44]:

$$\frac{C_e}{Q_e} = \frac{1}{Q_m} C_e + \frac{1}{K_L Q_m} \tag{3}$$

where Q_m (mg·g⁻¹) denotes the theoretical maximum adsorption capacity, Q_e (mg·g⁻¹) is the equilibrium adsorption capacity at the equilibrium concentration C_e (mg·L⁻¹) and K_L (L·mg⁻¹) means the Langmuir constant related to binding strength.

$$\ln Q_e = \frac{1}{n} \ln C_e + \ln K_F \tag{4}$$

where K_F ((mg·g⁻¹) (L·mg⁻¹)^{1/n}) refers to the Freundlich constant and $1/n$ represents the adsorption intensity [2].

$$\ln Q_e = \ln Q_m - k\varepsilon^2 \tag{5}$$

where Q_m refers to the calculated maximum adsorption capacity (mol·g⁻¹), Q_e (mol·g⁻¹) is the equilibrium adsorption capacity, k (mol²·kJ⁻²) denotes a constant related to the adsorption energy and ε is the Polanyi potential, which can be described by

$$\varepsilon = RT \ln \left(1 + \frac{1}{C_e} \right) \tag{6}$$

where R ($8.314 \text{ J}\cdot\text{mol}^{-1}\cdot\text{K}^{-1}$) represents the gas constant, T (K) is the absolute temperature and C_e ($\text{mol}\cdot\text{L}^{-1}$) denotes the equilibrium concentration.

The linear fitting of adsorption data by the Langmuir, Freundlich and Dubinin–Radushkevich models according to Equations (3)–(5), respectively, are exhibited in Figure 7 and the fitting results are listed in Table 9. It can be seen that the correlation coefficients (R^2) for the Langmuir model is 0.998, much higher than those for the Freundlich (0.760) and Dubinin–Radushkevich (0.741) models, indicating that the Langmuir model is more appropriate for describing the isothermal adsorption process when compared to the other two models. The theoretical maximum adsorption capacity ($29.33 \text{ mg}\cdot\text{g}^{-1}$) calculated on the basis of the Langmuir model is very close to the measured value ($31.05 \text{ mg}\cdot\text{g}^{-1}$), revealing that a monolayer adsorption of lead ions takes place homogeneously on the uniform and energetically identical active sites on the surface of slag adsorbent [2,45]. Another intrinsic parameter R_L , defined in Equation (7), is used to evaluate the Langmuir adsorption [46]:

$$R_L = \frac{1}{1 + K_L C_0} \quad (7)$$

where K_L and C_0 represent the Langmuir constant and the initial concentration of lead ions, respectively. It is generally believed that unfavorable adsorption, linear adsorption, favorable adsorption and irreversible adsorption occur in case of $R_L > 1$, $R_L = 1$, $0 < R_L < 1$ and $R_L = 0$, respectively. The R_L values in the present work range from 0.000651 to 0.009671, confirming a favorable adsorption [47]. The maximum adsorption capacity ($113.54 \text{ mg}\cdot\text{g}^{-1}$) obtained according to the Dubinin–Radushkevich (0.741) model deviates considerably from the measured value, further implying that the Dubinin–Radushkevich (0.741) model is not applicable for the adsorption.

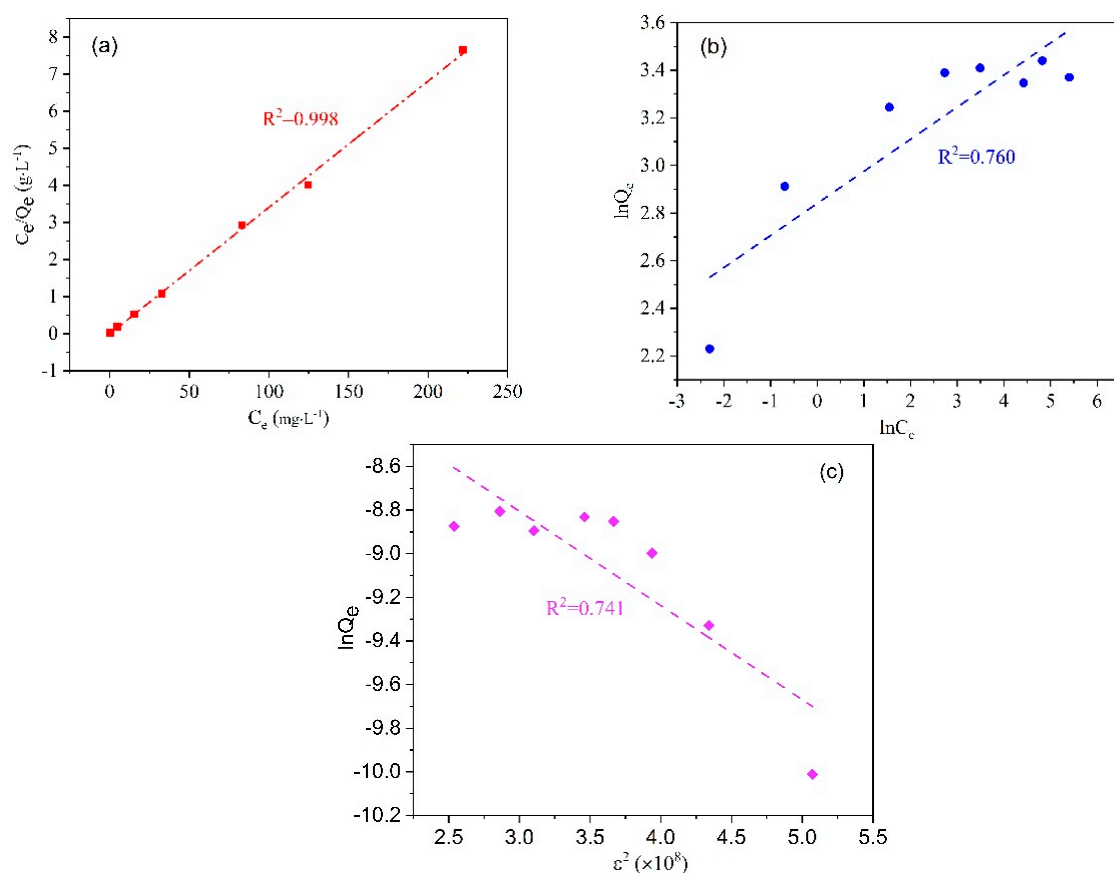


Figure 7. Linear fitting of Langmuir (a), Freundlich (b) and Dubinin–Radushkevich (c) isotherm for lead ion adsorption on pristine slag.

Table 9. Isothermal constants for the adsorption of lead ions on pristine slag.

Langmuir			Freundlich			Dubinin–Radushkevich		
Q_m ($\text{mg}\cdot\text{g}^{-1}$)	K_L ($\text{L}\cdot\text{mg}^{-1}$)	R^2	K_F ($(\text{mg}\cdot\text{g}^{-1})$ ($\text{L}\cdot\text{mg}^{-1}$) $^{1/n}$)	n	R^2	Q_m ($\text{mg}\cdot\text{g}^{-1}$)	k ($\text{mol}^2\cdot\text{kJ}^{-2}$)	R^2
29.33	5.12	0.998	17.12	7.42	0.760	113.54	0.432	0.741

3.2.4. Kinetics

Pseudo-first-order, pseudo-second-order and intraparticle diffusion models, denoted in Equations (8)–(10), respectively, were adopted to characterize the adsorption kinetics [24,48]:

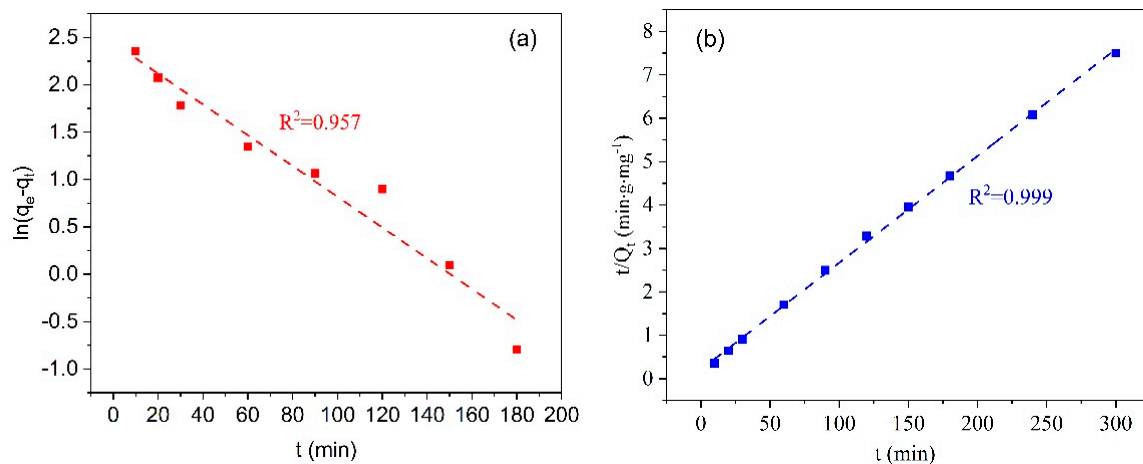
$$\ln(Q_e - Q_t) = \ln(Q_e) - k_1 t \quad (8)$$

$$\frac{t}{Q_t} = \frac{1}{k_2 Q_e^2} + \frac{t}{Q_e} \quad (9)$$

$$Q_t = k_i t^{1/2} + C \quad (10)$$

where Q_e ($\text{mg}\cdot\text{g}^{-1}$) and Q_t ($\text{mg}\cdot\text{g}^{-1}$) refer to the adsorption capacity at the reaction equilibrium and at each contact time t (min), respectively, k_1 (min^{-1}), k_2 ($\text{g}\cdot\text{mg}^{-1}\cdot\text{min}^{-1}$) and k_i ($\text{mg}\cdot\text{g}^{-1}\cdot\text{min}^{-1/2}$) represent the pseudo-first-order rate constant, pseudo-second-order rate constant and the intraparticle diffusion constant, respectively, and C is the intercept.

Figure 8 exhibits the linear fitting of adsorption data by pseudo-first-order, pseudo-second-order and intraparticle diffusion model based on Equations (8)–(10), respectively, and Table 10 lists the kinetic parameters, the equilibrium adsorption capacity (Q_e) and the regression coefficient (R^2). The R^2 value of pseudo-second-order model (0.999) is larger than those of pseudo-first-order (0.957) and intraparticle diffusion (0.921) model and the equilibrium adsorption capacity derived from pseudo-second-order kinetic equation ($40.62 \text{ mg}\cdot\text{g}^{-1}$) is much more similar to the experimental value ($38.55 \text{ mg}\cdot\text{g}^{-1}$), indicating that the pseudo-second-order model is more suitable for describing the adsorption of lead ions on the slag. This observation suggests that the limiting step in the adsorption is predominantly controlled by a chemical adsorption mechanism, in other words, electronic transfer and electronic sharing between the adsorbate and adsorbent are involved in the adsorption process [18,49,50]. Therefore, any strategies that may enhance the chemical interaction between lead ions and the superficial functional groups of the slag are highly advantageous to the removal efficiency of the lead ions from wastewater. This may be realized by grafting various functional groups that have great affinity toward lead ions on the surface of slag.

**Figure 8.** Cont.

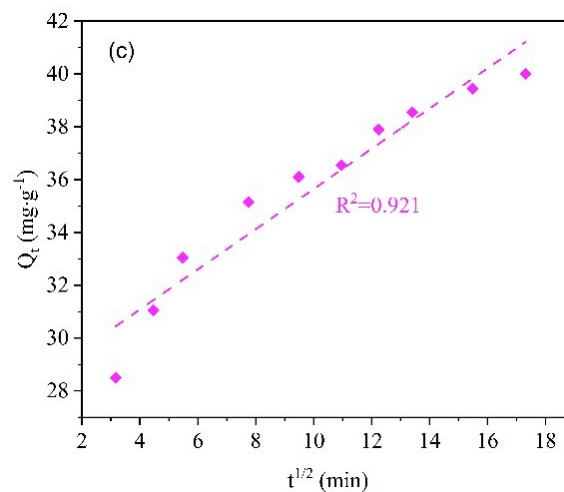


Figure 8. Linear fitting of pseudo-first-order (a), pseudo-second-order (b) and intraparticle diffusion (c) kinetic models for the lead ions adsorption on pristine slag.

Table 10. Kinetic parameters for the adsorption of lead ions on pristine slag.

Pseudo-First-Order			Pseudo-Second-Order			Intraparticle Diffusion		
Q_e (mg·g ⁻¹)	k_1 (mg ⁻¹)	R^2	Q_e (mg·g ⁻¹)	k_2 (g·mg ⁻¹ min ⁻¹)	R^2	k_i (mg·g ⁻¹ ·min ^{-1/2})	C	R^2
11.49	0.01624	0.957	40.62	0.00295	0.999	0.760	28.04	0.921

3.3. Lead Ion Removal by Aminopropyl-Modified Slag

As discussed in Section 3.2.1, the pristine slag becomes less effective for the adsorption of lead ions at high initial concentration. In this section, use of aminopropyl groups was attempted in order to modify the slag surface for the purpose of creating more compatible binding sites for lead ions by mean of post-grafting with APTES.

3.3.1. Effect of Modification Conditions on the Adsorption of Lead Ions

Three modification conditions, e.g., APTES concentration, modification time and modification temperature were investigated for their effect on the removal effectiveness of lead ions on the modified slag; the results are exhibited in Figure 9. The adsorption capacity increases significantly with increasing APTES concentration, reaching a maximum value of 68.35 mg·g⁻¹ at the APTES concentration of 25 wt%, and then decreases slightly upon higher APTES concentration (Figure 9a). It is generally accepted that surface modification is realized via the condensation reaction between the surface hydroxyl groups of slag and the ethoxy groups of APTES. After condensation, the surface hydroxyl groups are replaced by aminopropyl groups and this tendency is much more pronounced at higher APTES concentration. Previous work has demonstrated that aminopropyl groups are more affiliative to lead ions than hydroxyl groups [28,30]. That is why the adsorption capacity increases after surface functionalization with more aminopropyl groups. However, excess APTES may generate steric hindrance, which could prevent some hydroxyl groups from being accessible to APTES molecules, thus leading to the incomplete surface modification and the slight decrease of adsorption capacity. Figure 9b shows that the adsorption capacity increases sharply at the first 24 h and reaches a relatively saturated value 24 h later. The rapid increase of adsorption capacity at the initial stage can be ascribed to the successful grafting of aminopropyl groups on the surface. The surface hydroxyl groups are completely consumed 24 h later so that more aminopropyl groups are unable to link to the slag surface. As exhibited in Figure 9c, the adsorption capacity rises gradually with increasing temperatures from 20 to 40 °C, due to the possibility that the condensation

reaction between the hydroxyl groups and the APTES molecules are more favorable since the APTES molecules diffuse more rapidly in the solution at higher temperatures. A further increase of temperature to greater than 40 °C does not promote the adsorption capacity because no more hydroxyls groups are available for the residual APTES molecules. It is noted that the modification conditions have the same effect on the removal rate as that on adsorption capacity. The optimal modification conditions are obtained as follows: APTES concentration of 25 wt%, modification time of 36 h and modification temperature of 40 °C.

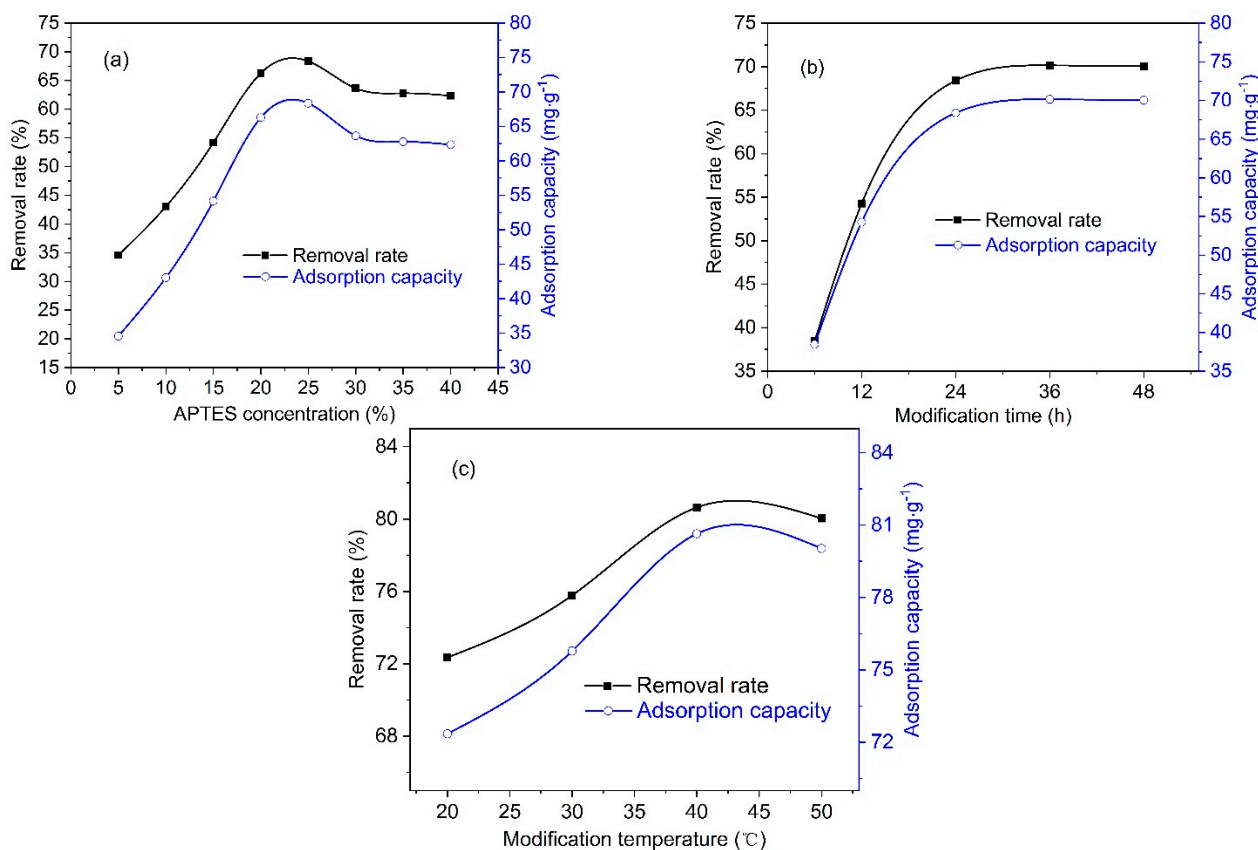


Figure 9. The effect of APTES concentration (a), modification time (b) and modification temperature (c) on the adsorption of lead ions on the modified slag.

3.3.2. Adsorption Mechanism

Figure 10 reveals the comparison of the adsorption performance between the pristine and modified slag. After modification by aminopropyl groups, the slag exhibits considerable enhancement of removal rate and adsorption capacity, from 20.71 to 64.32% and from 29.01 to 96.48 mg·g⁻¹, respectively, at a high lead ion initial concentration of 300 mg·L⁻¹. Table 11 compares the lead ions removal performance between our samples and various adsorbents reported in previous literature. Although the slags used in the present work exhibit adsorption performance inferior to that of the high-cost adsorbents [25,45,51–53], such as graphene, activated carbon, metal organic framework (MOF), among others, these slags are actually competitive to most of the adsorbents derived from agricultural and industrial wastes and natural minerals [11,13,48,54–59].

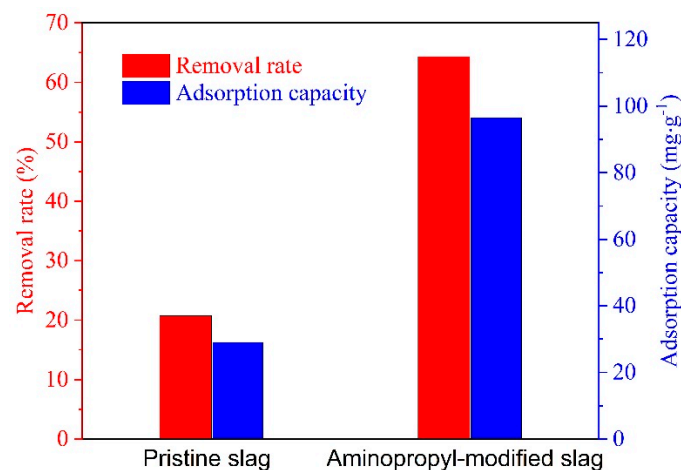


Figure 10. The comparison of the adsorption performance between the pristine and aminopropyl-modified slag.

Table 11. Comparison of the lead ion removal performance of various adsorbents.

Adsorbents	pH	T (°C)	CT (min)	IC (mg·L ⁻¹)	AD (g·L ⁻¹)	AC (mg·g ⁻¹)	RA (%)	Refs.
Iron/reduced graphene oxide composites	5.0	21	60	400	0.6	910.00	100.00	[51]
Mesoporous silica-grafted graphene oxide	5.0	25	10	150	0.3	255.10	99.00	[52]
Activated carbon	2.0	RT	1440	100	1.0	294.00	73.00	[53]
Fe ₃ O ₄ decorated MOF	4.0	25	1440	500	1.0	610.00	93.00	[45]
Polyacrylonitrile beads	7.0	30	180	400	5.0	145.00	-	[25]
Sugar beet pulp	5.0	25	70	207	8.0	43.50	71.00	[54]
Raw coconut husk	7.0	-	-	50	2.5	21.20	-	[55]
Electrolytic manganese residues	5.0	25	180	21	0.5	119.90	91.00	[13]
Bentonite	6.0	20	250	500	10.0	58.00	91.10	[56]
Montmorillonite	6.0	25	100	500	10.0	3.25	90.00	[57]
Blast furnace slag	6.5	25	-	5	0.1–20.0	4.90	79.00	[58]
Steel furnace slag	5.5	RT	1440	1	0.6	6.60	34.00	[11]
Desulfurization slag	6.0	23	90	180	40.0	130.20	98.80	[48]
Al(OH) ₃ -modified nickel slag	6.0	25	720	50	40.0	1.60	99.60	[59]
Blast furnace slag	7.0	60	120	40	2.0	49.99	99.98	This work
Blast furnace slag	6.0	20	60	300	2.0	29.01	20.70	This work
NH ₂ -modified slag	6.0	20	60	300	2.0	96.50	64.30	This work

Note: T = temperature; RT = room temperature; CT = contact time; IC = initial lead ion concentration; AD = adsorbent dose; AC = adsorption capacity; RA = removal rate.

As illustrated in Figure 11, for the pristine slag, surface hydroxyl groups are responsible for the lead ion adsorption. The lone pair electrons in the oxygen atoms of hydroxyl groups play a critical role in the complexation between the lead ions and hydroxyl groups. After modification, aminopropyl group behaves as a substitute for hydroxyl group [28–30]. There are also lone pair electrons in the nitrogen atom of aminopropyl group, and thus the aminopropyl group can be considered as a nucleophilic species. The nucleophilicity usually comes from alkalinity and polarizability. It is obvious that the alkalinity of the amino group is stronger than that of hydroxyl groups, but the polarizability of both groups is extremely similar since both N and O atoms are located in the second period of the periodic table, and therefore the aminopropyl group is more nucleophilic than the hydroxyl group. As a result, the aminopropyl groups are more inclined to form a complex with lead ions than hydroxyl groups [28–30], thus leading to a superior adsorption performance for the modified slag compared to the pristine slag. Additionally, the extremely tiny BET surface area and pore volume of the slag indicate that the lead ion adsorption on the slag

is determined by the external surface rather than the porosity (in other words, the inner surface). The physical adsorption can be ignored for the slag.

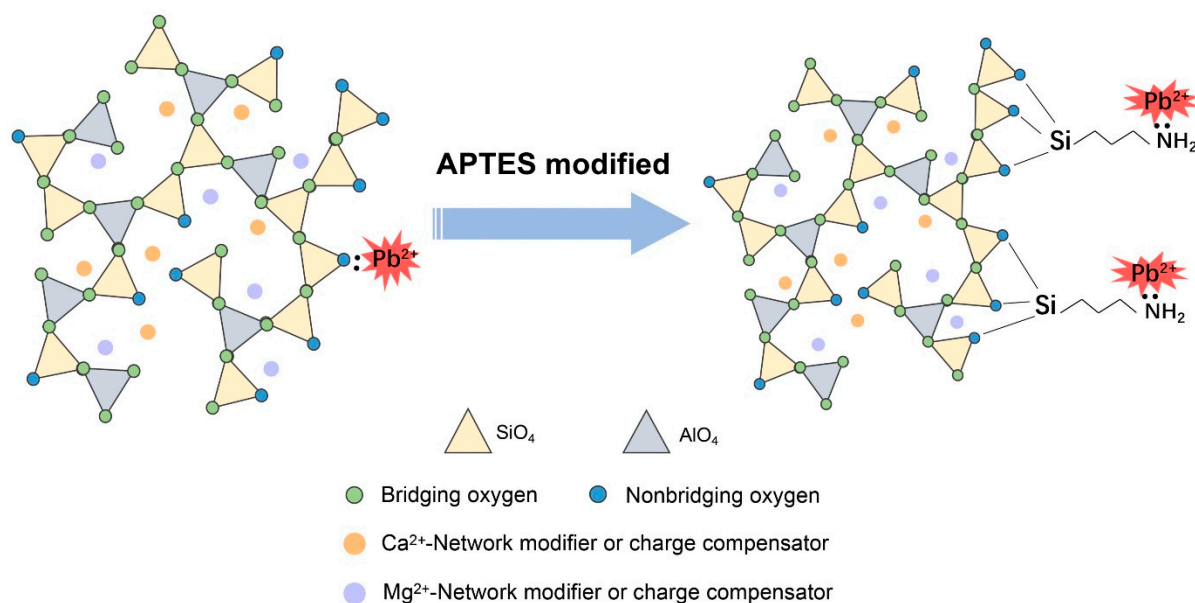


Figure 11. The proposed lead ion adsorption mechanism on the pristine and aminopropyl-modified slag.

4. Conclusions

The present work aims to investigate the lead ions adsorption behavior of blast furnace slag and proposes a strategy to improve the lead ion removal performance. The blast furnace slag, mainly composed of SiO_2 , CaO , Al_2O_3 and MgO , has an amorphous structure in which SiO_4 and AlO_4 tetrahedra constitute the basic building blocks of the networks. The hydroxyl groups on SiO_4 tetrahedra endow the slag with ability to adsorb lead ions in wastewater. The pristine slag has an adsorption capacity of $49.99 \text{ mg}\cdot\text{g}^{-1}$ and a removal rate of 99.98% for lead ions under the following conditions: pH of 7, adsorption temperature of 60°C , contact time of 120 min and initial lead ion concentration of $40 \text{ mg}\cdot\text{L}^{-1}$; the residual concentration of lead ions in the solution after adsorption is less than $1 \text{ mg}\cdot\text{L}^{-1}$, which is close to the national emission standard. The Langmuir model (correlation coefficient, $R^2 = 0.998$) fits the adsorption data better than the Freundlich model ($R^2 = 0.760$). The pseudo-second-order model is more suitable for describing the experimental data than pseudo-first-order model, indicating that lead ions are predominately removed by chemical adsorption. Surface modification with aminopropyl groups enhances the adsorption performance of lead ions from aqueous solution with a high lead ion concentration of $300 \text{ mg}\cdot\text{L}^{-1}$. For the modified slag, the removal rate of lead ions considerably increases from 20.71 to 64.32% and the adsorption capacity significantly increases from 29.01 to $96.48 \text{ mg}\cdot\text{g}^{-1}$. In future research, it will be necessary to develop lower-cost surface modification agents, which are currently unaffordable for large scale application.

Author Contributions: Conceptualization, Q.W.; methodology, Y.W., H.L. and S.C.; formal analysis, Y.W. and H.L.; investigation, Y.W., H.L. and S.C.; resources, Q.W.; data curation, Y.W., H.L. and S.C.; writing—original draft preparation, Y.W. and Q.W.; writing—review and editing, Q.W.; supervision, Q.W.; project administration, Q.W.; funding acquisition, Q.W. All authors have read and agreed to the published version of the manuscript.

Funding: This research was funded by the National Key Research and Development Program of China, grant number 2017YFB0603601-03 and the National Natural Science Fund for Innovative Research Groups, grant number 51621003.

Conflicts of Interest: The authors declare no conflict of interest.

References

1. Bouabidi, Z.B.; El-Naas, M.H.; Cortes, D.; McKay, G. Steel-Making dust as a potential adsorbent for the removal of lead (II) from an aqueous solution. *Chem. Eng. J.* **2018**, *334*, 837–844. [[CrossRef](#)]
2. Kumara, G.M.P.; Kawamoto, K.; Saito, T.; Hamamoto, S.; Asamoto, S. Evaluation of autoclaved aerated concrete fines for removal of Cd(II) and Pb(II) from Wastewater. *J. Environ. Eng.* **2019**, *145*, 1943–7870. [[CrossRef](#)]
3. Momcilovic, M.; Purenovic, M.; Bojic, A.; Zarubica, A.; Randelovic, M. Removal of lead(II) ions from aqueous solutions by adsorption onto pine cone activated carbon. *Desalination* **2011**, *276*, 53–59. [[CrossRef](#)]
4. Lu, D.; Cao, Q.; Cao, X.; Luo, F. Removal of Pb(II) using the modified lawn grass: Mechanism, kinetics, equilibrium and thermodynamic studies. *J. Hazard. Mater.* **2009**, *166*, 239–247. [[CrossRef](#)]
5. Matlock, M.M.; Howerton, B.S.; Atwood, D.A. Chemical precipitation of heavy metals from acid minedrainage. *Water Res.* **2002**, *36*, 4757–4764. [[CrossRef](#)]
6. Alyüz, B.; Veli, S. Kinetics and equilibrium studies for the removal of nickel and zinc from aqueous solutions by ion exchange resins. *J. Hazard. Mater.* **2009**, *167*, 482–488. [[CrossRef](#)] [[PubMed](#)]
7. Raffin, M.; Germain, E.; Judd, S. Wastewater polishing using membrane technology: A review of existing installations. *Environ. Technol.* **2012**, *34*, 617–627. [[CrossRef](#)] [[PubMed](#)]
8. Chan, B.K.C.; Dudeney, A.W.L. Reverse osmosis removal of arsenic residues from bioleaching of refractory gold concentrates. *Miner. Eng.* **2008**, *21*, 272–278. [[CrossRef](#)]
9. Mahar, A.; Wang, P.; Ali, A.; Kumar, A.M.; Hussain, L.A.; Wang, Q.; Li, R.; Zhang, Z. Challenges and opportunities in the phytoremediation of heavy metals contaminated soils: A review. *Ecotoxicol. Environ. Saf.* **2016**, *126*, 111–121. [[CrossRef](#)] [[PubMed](#)]
10. Medina, T.J.; Arredondo, S.P.; Corral, R.; Jacobo, A.; Zárraga, R.A.; Rosas, C.A.; Cabrera, F.G.; Bernal, J.M. Microstructure and Pb²⁺ Adsorption Properties of Blast Furnace Slag and Fly Ash based Geopolymers. *Minerals* **2020**, *10*, 808. [[CrossRef](#)]
11. Mercado-Borrayo, B.M.; Contreras, R.; Sánchez, A.; Font, X.; Schouwenaars, R.; Ramírez-Zamora, R.M. Optimisation of the removal conditions for heavy metals from water: A comparison between steel furnace slag and CeO₂ nanoparticles. *Arab. J. Chem.* **2020**, *13*, 1712–1719. [[CrossRef](#)]
12. Zahar, M.S.; Kusin, F.M.; Mohamed, K.N.; Masri, N. Treatment of acid mine drainage (AMD) using industrial by-product: Sorption behavior of steel slag for metal-rich mine water. *Glob. Nest. J.* **2020**, *22*, 258–267.
13. Ma, M.; Du, Y.; Bao, S.; Li, J.; Wei, H.; Lv, Y.; Song, X.; Zhang, T.; Du, D. Removal of cadmium and lead from aqueous solutions by thermal activated electrolytic manganese residues. *Sci. Total Environ.* **2020**, *748*, 141490. [[CrossRef](#)] [[PubMed](#)]
14. Ahmed, J.K.; Ahmaruzzaman, M. A review on potential usage of industrial waste materials for binding heavy metal ions from aqueous solutions. *J. Water Process. Eng.* **2016**, *10*, 39–47. [[CrossRef](#)]
15. Abbas, A.; Al-Amer, A.M.; Laoui, T.; Al-Marri, M.J.; Nasser, M.S.; Khraisheh, M.; Atieh, M.A. Heavy metal removal from aqueous solution by advanced carbon nanotubes: Critical review of adsorption applications. *Sep. Purif. Technol.* **2016**, *157*, 141–161.
16. Gao, Y.; Jiang, J.; Tian, S.; Li, K.; Yan, F.; Liu, N.; Yang, M.; Chen, X. BOF steel slag as a low-cost sorbent for vanadium (V) removal from soil washing effluent. *Sci. Rep.* **2017**, *7*, 11177. [[CrossRef](#)] [[PubMed](#)]
17. Leiviskä, T.; Khalid, M.K.; Sarpola, A.; Tanskanen, J. Removal of vanadium from industrial wastewater using iron sorbents in batch and continuous flow pilot systems. *J. Environ. Manag.* **2017**, *190*, 231–242. [[CrossRef](#)]
18. Azamfire, B.; Bulgariu, D.; Bulgariu, L. Efficient removal of toxic metal ions (Pb(II) and Hg(II) ions in single component systems by adsorption on romanian clay material. *Rev. Chim.* **2020**, *71*, 37–47. [[CrossRef](#)]
19. Ali, A.; Saeed, K.; Mabood, F. Removal of chromium (VI) from aqueous medium using chemically modified banana peels as efficient low-cost adsorbent. *Alex. Eng. J.* **2016**, *55*, 2933–2942. [[CrossRef](#)]
20. Módenes, A.N.; Espinoza-Quñones, F.R.; Colombo, A.; Geraldini, C.L.; Trigueros, D.E.G. Inhibitory effect on the uptake and diffusion of Cd²⁺ onto soybean hull sorbent in Cd-Pb binary sorption systems. *J. Environ. Manag.* **2015**, *154*, 22–32. [[CrossRef](#)]
21. Lavecchia, R.; Medici, F.; Patterer, S.; Zuorro, A. Lead removal from water by adsorption on spent coffee grounds. *Chem. Eng. Trans.* **2016**, *47*, 295–300.
22. Czech, B.; Hojamberdiev, M.; Bogusz, A. Impact of thermal treatment of calcium silicate-rich slag on the removal of cadmium from aqueous solution. *J. Clean. Prod.* **2018**, *200*, 369–379. [[CrossRef](#)]
23. Yusuf, M.; Chuah, L.; Khan, M.A.; Choong, T.S.Y. Adsorption of nickel on electric arc furnace slag: Batch and column studies. *Sep. Sci. Technol.* **2014**, *49*, 388–397. [[CrossRef](#)]
24. Zhan, X.; Xiao, L.; Liang, B. Removal of Pb(II) from acid mine drainage with bentonite-steel slag composite particles. *Sustainability* **2019**, *11*, 4476. [[CrossRef](#)]
25. Bhunia, P.; Chatterjee, S.; Rudra, P.; De, S. Chelating polyacrylonitrile beads for removal of lead and cadmium from wastewater. *Sep. Purif. Technol.* **2018**, *193*, 202–213. [[CrossRef](#)]
26. Xu, G.; Xie, Y.; Cao, J.; Tao, M.; Zhang, W.Q. Highly selective and efficient chelating fiber functionalized by bis(2-yrityldimethyl)amino group for heavy metal ions. *Polym. Chem.* **2016**, *7*, 3874–3883. [[CrossRef](#)]
27. Deng, S.B.; Bai, R.B.; Chen, J.P. Aminated polyacrylonitrile fibers for lead and copper removal. *Langmuir* **2003**, *19*, 5058–5064. [[CrossRef](#)]
28. Tang, Y.; Liang, S.; Wang, J.; Yu, S.; Wang, Y. Amino-functionalized core-shell magnetic mesoporous composite microspheres for Pb(II) and Cd(II) removal. *J. Environ. Sci.* **2013**, *25*, 830–837. [[CrossRef](#)]

29. Zou, B.F.; Chen, K.; Wang, Y.Q.; Niu, C.Y.; Zhou, S.M. Amino-functionalized magnetic magnesium silicate double-shelled hollow microspheres for enhanced removal of lead ions. *RSC Adv.* **2015**, *5*, 22973–22979. [[CrossRef](#)]
30. Ji, L.Q.; Zhou, L.C.; Bai, X.; Shao, Y.M.; Zhao, G.H.; Qu, Y.Z.; Wang, C.; Li, Y.F. Facile synthesis of multiwall carbon nanotubes/iron oxides for removal of tetrabromobisphenol A and Pb(II). *J. Mater. Chem.* **2012**, *22*, 15853–15862. [[CrossRef](#)]
31. Zhu, C.; Hu, T.; Tang, L.; Zeng, G.; Deng, Y.; Lu, Y.; Fang, S.; Wang, J.; Liu, Y.; Yu, J. Highly efficient extraction of lead ions from smelting wastewater, slag and contaminated soil by two-dimensional montmorillonite-based surface ion imprinted polymer absorbent. *Chemosphere* **2018**, *209*, 246–257. [[CrossRef](#)]
32. Nie, S.; Thomsen, R.M.; Skibsted, J. Impact of Mg substitution on the structure and pozzolanic reactivity of calcium aluminosilicate (CaO-Al₂O₃-SiO₂) glasses. *Cem. Concr. Res.* **2020**, *138*, 106231. [[CrossRef](#)]
33. Paul, G.; Bisio, C.; Braschi, I.; Cossi, M.; Gatti, G.; Gianotti, E.; Marchese, L. Combined solid-state NMR, FT-IR and computational studies on layered and porous materials. *Chem. Soc. Rev.* **2018**, *47*, 5684–5739. [[CrossRef](#)] [[PubMed](#)]
34. Li, F.; Liu, L.; Yang, Z.; Li, S. Influence of modified multi-walled carbon nanotubes on the mechanical behavior and toughening mechanism of an environmentally friendly granulated blast furnace slag-based geopolymer matrix. *Ceram. Int.* **2021**, *47*, 907–922. [[CrossRef](#)]
35. Zhang, J.; Tan, H.; Cai, L.; He, X.; Yang, W.; Liu, X. Ultra-fine slag activated by sodium carbonate at ambient temperature. *Constr. Build. Mater.* **2020**, *264*, 120695. [[CrossRef](#)]
36. Lin, L.; Yu, Y. Adsorption of Pb²⁺ and Cu²⁺ with unburned desulphurization slag modified nickel slag. *Chin. J. Struct. Chem.* **2017**, *36*, 491–502.
37. Zheng, P.; Li, X.; Wu, J.; Wang, N.; Li, J.; An, Q. Enhanced butanol selectivity of pervaporation membrane with fluorinated monolayer on polydimethylsiloxane surface. *J. Membr. Sci.* **2018**, *548*, 215–222. [[CrossRef](#)]
38. Eunhee, P.; Jaehyun, H. Three-dimensionally interconnected porous PDMS decorated with poly(dopamine) and Prussian blue for floatable, flexible, and recyclable photo-Fenton catalyst activated by solar light. *Appl. Surf. Sci.* **2021**, *545*, 148990.
39. Li, X.; Cao, M.; Shan, H.; Tezel, F.H.; Li, B. Facile and scalable fabrication of superhydrophobic and superoleophilic PDMS-co-PMHS coating on porous substrates for highly effective oil/water separation. *Chem. Eng. J.* **2019**, *358*, 1101–1113. [[CrossRef](#)]
40. Calzaferri, G.; Gallagher, S.H.; Brühwiler, D. Entropy in multiple equilibria. Argon and nitrogen adsorption isotherms of nonporous, microporous, and mesoporous materials. *Microporous Mesoporous Mater.* **2021**, *312*, 110744. [[CrossRef](#)]
41. Colmenares-Zerpa, J.; Chimentão, R.J.; Gispert-Guirado, F.; Peixoto, A.F.; Llorca, J. Preparation of SBA-15 and Zr-SBA-15 materials by direct-synthesis and pH-adjustment methods. *Mater. Lett.* **2021**, *301*, 130326. [[CrossRef](#)]
42. Zhang, X.; Wu, Y.; Li, X.; Meng, X.; Shi, H.; Wu, Z.; Zhang, J. Preparation of mesoporous silica from coal slag and its metal ion adsorption behavior. *Korean J. Chem. Eng.* **2019**, *36*, 753–762. [[CrossRef](#)]
43. Almási, A.; Omid, M.; Khodadadian, M.; Khamutian, R.; Gholivand, M.B. Lead(II) and cadmium(II) removal from aqueous solution using processed walnut shell: Kinetic and equilibrium study. *Toxicol. Environ. Chem.* **2012**, *94*, 660–671. [[CrossRef](#)]
44. Mouni, L.; Merabet, D.; Bouzaza, A.; Belkhir, L. Adsorption of Pb(II) from aqueous solutions using activated carbon developed from Apricot stone. *Desalination* **2011**, *276*, 148–153. [[CrossRef](#)]
45. Goyal, P.; Tiwary, C.S.; Misra, S.K. Ion exchange based approach for rapid and selective Pb (II) removal using iron oxide decorated metal organic framework hybrid. *J. Environ. Manag.* **2021**, *277*, 111469. [[CrossRef](#)]
46. Hall, K.; Eagleton, L.; Acrivos, A.; Vermeulen, T. Pore-and solid-diffusion kinetics in fixed-bed adsorption under constant-pattern conditions. *Ind. Eng. Chem. Fundam.* **1996**, *5*, 212–223. [[CrossRef](#)]
47. Mckay, G.; Blair, H.S.; Gardener, J.R. Adsorption of dyes on chitin I. Equilibrium studies. *J. Appl. Polym. Sci.* **1982**, *27*, 3043–3057. [[CrossRef](#)]
48. Wu, Q.; You, R.; Clark, M.; Yu, Y. Pb(II) removal from aqueous solution by a low-cost adsorbent dry desulfurization slag. *Appl. Surf. Sci.* **2014**, *314*, 129–137. [[CrossRef](#)]
49. Ho, Y. Review of second-order models for adsorption systems. *J. Hazard. Mater.* **2006**, *136*, 681–689. [[CrossRef](#)] [[PubMed](#)]
50. Yang, L.; Yang, M.; Xu, P.; Zhao, X.; Bai, H.; Li, H. Characteristics of nitrate removal from aqueous solution by modified steel slag. *Water* **2017**, *9*, 757. [[CrossRef](#)]
51. Fan, M.; Li, T.; Hu, J.; Cao, R.; Wu, Q.; Wei, X.; Li, L.; Shi, X.; Ruan, W. Synthesis and characterization of reduced graphene oxide-supported nanoscale zero-valent iron (nZVI/rGO) composites used for Pb (II) removal. *Materials* **2016**, *9*, 687. [[CrossRef](#)] [[PubMed](#)]
52. Li, X.; Wang, Z.; Li, Q.; Ma, J.; Zhu, M. Preparation, characterization, and application of mesoporous silica-grafted graphene oxide for highly selective lead adsorption. *Chem. Eng. J.* **2015**, *273*, 630–637. [[CrossRef](#)]
53. Karnib, M.; Kabbani, A.; Holail, H.; Olama, Z. Heavy metals removal using activated carbon, silica and silica activated carbon composite. *Energy Procedia.* **2014**, *50*, 113–120. [[CrossRef](#)]
54. Pehlivan, E.; Yanik, B.H.; Ahmetli, G.; Pehlivan, M. Equilibrium isotherm studies for the uptake of cadmium and lead ions onto sugar beet pulp. *Bioresour. Technol.* **2008**, *99*, 3520–3527. [[CrossRef](#)]
55. Sewwandi, B.G.N.; Vithanage, M.; Wijesekara, S.S.R.M.D.H.R.; Mowjood, M.I.M.; Hamamoto, S.; Kawamoto, K. Adsorption of Cd (II) and Pb (II) onto humic acid-treated coconut (Cocos nucifera) husk. *J. Hazard. Toxic Radioact. Waste* **2014**, *18*, 04014001. [[CrossRef](#)]
56. Galindo, L.S.G.; Almeida Neto, A.F.D.; Silva, M.G.C.D.; Vieira, M.G.A. Removal of cadmium (II) and lead (II) ions from aqueous phase on sodic bentonite. *Mater. Res.* **2013**, *16*, 515–527. [[CrossRef](#)]

57. Abdellaoui, Y.; Olgúin, M.T.; Abatal, M.; Ali, B.; Méndez, S.E.D.; Santiago, A.A. Comparison of the divalent heavy metals (Pb, Cu and Cd) adsorption behavior by montmorillonite-KSF and their calcium-and sodium-forms. *Superlattices Microstruct.* **2019**, *127*, 165–175. [[CrossRef](#)]
58. Nguyen, T.C.; Loganathan, P.; Nguyen, T.V.; Kandasamy, J.; Naidu, R.; Vigneswaran, S. Adsorptive removal of five heavy metals from water using blast furnace slag and fly ash. *Environ. Sci. Pollut. Res.* **2018**, *25*, 20430–20438. [[CrossRef](#)]
59. Liang, L.; Yan, Y. Application of modified nickel slag adsorbent on the removal of Pb²⁺ and Cu²⁺ from aqueous solution. *Chin. J. Struct. Chem.* **2016**, *35*, 879–888.